Spin effects in high-energy proton-proton scattering within a diquark model

S. V. Goloskokov*
Bogoliubov Laboratory of Theoretical Physics, Joint Institute for Nuclear Research, Dubna 141980, Moscow region, Russia

P. Kroll†
Fachbereich Physik, Universität Wuppertal, D-42097 Wuppertal, Germany

(Received 31 July 1998; revised manuscript received 27 January 1999; published 14 June 1999)

We study pp scattering at high energies and moderately large momentum transfer, using a model in which the proton is viewed as being composed of a quark and a diquark. We show that this model leads to single and double spin transverse asymmetries which are neither small nor vanish at high energies.
[S0556-2821(99)03313-5]

PACS number(s): 12.38.Bx, 13.85.Dz, 13.88.+e

I. INTRODUCTION

The adequate theoretical description of spin effects in high-energy exclusive processes at moderately large momentum transfer is one of the unsolved problems in QCD. As is well known, massless QCD leads to hadronic helicity conservation and, hence, to zero single-spin asymmetries. Mass and higher order perturbative QCD corrections lead to nonvanishing single-spin transverse asymmetries:

$$A_N \propto m\alpha_s/\sqrt{-t}. \tag{1}$$

A QCD analysis reveals that the mass parameter m appearing in Eq. (1) is of the order of the hadron mass [1] and should not be interpreted as a current quark mass. So, one may expect a substantial single-spin asymmetry for momentum transfer $-t$ of the order of a few GeV^2. Actual estimates within QCD inspired models provide only values of the order of a few percent for single-spin asymmetries, indeed much smaller than the experimental results.

Experimentally, there are many observations of large spin effects at high energies and moderately large momentum transfer [2]. Sizable differences between the cross sections for different spin orientations of the initial state protons as well as large double-spin A_{NN} and single-spin A_N transverse asymmetries have been observed in the BNL experiment [3] for beam momenta p_B less than 28 GeV. The Fermilab experiment [4] finds values for A_N of about 10–20 % at $p_B = 200$ GeV and momentum transfers $|t| \geqslant 2$ GeV^2. This result is of the same order of magnitude as the BNL asymmetry at $p_B = 28$ GeV and similar values of t. Combining these observations with corresponding ones made at small momentum transfers [5], one is lead to the conclusion that spin effects in high-energy reactions exhibit a weak energy dependence.

Elastic scattering at high energies and fixed momentum transfer ($|t|/s$ small) is customarily believed to be under the control of the t-channel color-singlet Pomeron (and, eventually odderon) exchange that has a dominant nonflip coupling. The observed spin effects thus seem to require the existence of an additional Pomeron-like exchange in the helicity-flip amplitudes that has—up to eventual $\ln s$ factors—the same energy dependence as the standard Pomeron but is not in phase with it. Within QCD the Pomeron is interpreted as the t channel exchange of gluons with a total charge conjugation of unity ($C = +1$). Present attempts to understand it theoretically are based on the simple two-gluon picture for this object [6]. It is important to note that in such models the Pomeron couples to quarks and not directly to the hadrons. According to the model [7], the gluons representing the Pomeron preferentially interact with the same quark within a given hadron. As a consequence of this property, the Pomeron effectively couples to the hadron like an $C = +1$ isoscalar photon [7] and approximately reproduces the salient features of the additive quark model. In the Landshoff-Nachtmann (LN) nonperturbative model [8], the two gluons representing the Pomeron do not only couple to one and the same constituent. However, neither the LN model [8] nor that of [7] provides a spin-dependent Pomeron coupling. The question of gauge invariance for the models [7,8] has been investigated by Diehl [9].

In several models high energy spin effects have been investigated. Thus, for instance, in [10] the spin-dependent quark-Pomeron coupling was constructed from a gluon-loop contribution. It was shown that this quark-Pomeron coupling leads to fairly large spin asymmetries in diffractive quark-antiquark pair production and exhibits only a weak energy dependence [11]. In [12] rotating matter inside the proton was claimed to be the origin of spin effects. The authors of [13] considered the Pomeron interaction with the light quark-antiquark cloud of the proton. While these models provide spin effects at high energies in fair agreement with experiment they suffer from the large number of adjustable parameters they depend on. Moreover, the applicability of these models is restricted to small momentum transfer.

Here, in this work, we are interested in spin effects at high energies and moderately large momentum transfer (3 GeV$^2 < |t| \ll s$). In view of the polarization physics programs proposed for the future proton accelerators [14] this kinematical region is of topical interest. Our approach is based on the diquark picture [15] where the proton is viewed as being composed of a quark and a diquark in the dominant valence Fock state instead of three quarks. The diquarks represent an effective description of nonperturbative effects; their com-

*Email address: goloskkv@thsun1.jinr.dubna.su
†Email address: kroll@theorie.physik.uni-wuppertal.de

posite nature is taken into account by diquark form factors. The diquark picture of the proton simplifies our calculations drastically due to the reduced number of constituents. The combination of the quark-diquark picture of the proton and the hard scattering approach developed by Brodsky and Lepage [16] leads to successful descriptions of electromagnetic form factors and other exclusive reactions [17,18] at a fairly large momentum transfer. Spin effects are generated from spin 1 (vector) diquarks in that model. The model also provides phase differences between different helicity amplitudes in some cases and can therefore account for single-spin asymmetries in principle. Note, that these corrections are non-Pomeron-like because of the phase shift between the flip and nonflip contributions. However, even within the diquark model which is much simpler to handle than the three-quark picture of the proton, a full hard scattering analysis of elastic proton-proton scattering is beyond feasibility at present (see, for instance, [19]). Therefore, in order to simplify and in regard to the fact that we are not interested in the real hard scattering region for which the diquark model was originally designed, we use that model in combination with the two-gluon exchange picture as a representative of the Pomeron. We calculate the helicity-flip amplitude explicitly in that framework while, at the end, the nonflip amplitudes are described by a standard phenomenological Pomeron exchange. We note that Ramsey and Sivers [20] also proposed a hard scattering model that produces substantial spin effects. This model is based on quark-exchange and the Landshoff pinch contribution [21] to the pp helicity amplitudes.

In Sec. II we begin with a few kinematical preliminaries. A brief description of the diquark model is presented in Sec. III. The general structure of the various diquark contributions to elastic pp scattering is discussed in Sec. IV. In Sec. V we present our numerical results for spin asymmetries in elastic pp scattering and compare them to experimental data. Concluding remarks are given in Sec. VI.

II. PROTON-PROTON SCATTERING AT HIGH ENERGIES

The momenta and the Mandelstam variables of elastic proton-proton scattering are defined by

$$p(p_1)+p(p_2)\to p(p_3)+p(p_4) \tag{2}$$

and

$$s=(p_1+p_2)^2, \quad t=(p_1-p_3)^2.$$

Elastic pp scattering can be described in terms of helicity amplitudes

$$T_{\lambda_4\lambda_3;\lambda_2\lambda_1}=\bar{u}(p_4,\lambda_4)\bar{u}(p_3,\lambda_3)\hat{T}(s,t)u(p_2,\lambda_2)u(p_1,\lambda_1), \tag{3}$$

of which only five are independent. In Eq. (3) u denotes the spinor of a proton with momentum p_i and helicity λ_i. In the kinematical region of interest the double helicity-flip amplitudes are believed to be much smaller than the helicity nonflip ones and the two nonflip amplitudes are of equal magnitude approximately. These properties hold in most of models (see, for instance, [12,13]) and we will assume that they also hold in our approach. In this situation we can, for convenience and without loss of generality, fix the helicities of the protons 1 and 3 at $+1/2$. Therefore, we have to model a nonflip, F_{++}, and a flip amplitude, F_{+-}, only. F_{++} represents the average of the two nonflip amplitudes. There is no need for antisymmetrization of the amplitudes since the $p_3\leftrightarrow p_4$ interchanged contribution is suppressed by inverse powers of s in the kinematical region of interest ($t\leftrightarrow u\simeq s$).

In terms of the amplitudes F_{++} and F_{+-} the differential cross section is given by

$$\frac{d\sigma}{dt}=\frac{1}{64\pi s^2}[|F_{++}|^2+2|F_{+-}|^2]. \tag{4}$$

The single-spin asymmetry reads

$$A_N=-2\frac{\mathrm{Im}[F_{++}F_{+-}^*]}{|F_{++}|^2+2|F_{+-}|^2}, \tag{5}$$

while the double spin transverse asymmetry is given by

$$A_{NN}=2\frac{|F_{+-}|^2}{|F_{++}|^2+2|F_{+-}|^2}. \tag{6}$$

The A_{NN} asymmetry is related to the differential cross sections in parallel and anti-parallel spin states by

$$\frac{d\sigma(\uparrow\uparrow)/dt}{d\sigma(\uparrow\downarrow)/dt}=\frac{1+A_{NN}}{1-A_{NN}}. \tag{7}$$

In the following we are going to calculate the leading contribution to the helicity-flip amplitude within the diquark model, omitting corrections like m^2/t. The nonflip amplitude, on the other hand, is modeled by a phenomenological ansatz. As a crossing-even exchange grows $\propto s$, the Pomeron contribution is dominantly imaginary with only a very small real part suppressed by $1/s$ as follows from analyticity [22]. We will make use of two alternative parametrizations valid for $|t|$ larger then 3 GeV^2 (after the dip region of the differential cross section). Following, for instance, the authors of [13], we parametrize F_{++} as an exponential

$$F_{++}(s,t)=isb\exp(-a\sqrt{|t|}). \tag{8}$$

This ansatz is understood as being a consequence of multiple Pomeron exchange (MPE). Alternatively, we use the parametrization

$$F_{++}(s,t)=is\frac{c}{t^4}, \tag{9}$$

which may be viewed as a phenomenological version of the Landshoff pinch contribution (LP) [21] to pp scattering. Note, that the model results [13,21] confirm the imaginary of the amplitudes (8,9). In our numerical estimations we shall use the MPE fit for $b=45.967$ GeV^{-2}, $a=3.745$ GeV^{-1}, and

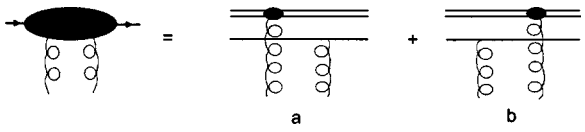

FIG. 1. Structure of the spin-nonflip proton vertex.

the LP fit for $c=6.284\ \mathrm{GeV}^6$. Both the parametrizations, Eqs. (8) and (9), describe rather well the pp differential cross section data at CERN Intersecting Storage Rings (ISR) energies [23]. An eventual residual energy dependence of the experimental data (perhaps of $\ln s$ type) will be ignored here. It is irrelevant for our purpose of investigating spin effects.

III. THE DIQUARK MODEL

As we said in the introduction we will make use of the diquark model of the proton advocated in [15,17,18]. Here we give a brief description of that model. In the hard scattering approach proposed by Brodsky and Lepage [16] the process $pp\to pp$ is expressed by a convolution of distribution amplitudes (DA) with hard-scattering amplitudes calculated in collinear approximation within perturbative QCD. In a collinear situation in which intrinsic transverse momenta are neglected and all constituents of a hadron have momenta parallel to each other and parallel to the momentum of the parent hadron, one may write the valence Fock state of the proton in a covariant fashion (omitting color indices for convenience):

$$|p,\lambda:qS;qV,\alpha\rangle = f_S\varphi_S(x_1)B_S u(p,\lambda) + f_V\varphi_V(x_1) \times B_V(\gamma^\alpha + p^\alpha/m)\gamma_5 u(p,\lambda)/\sqrt{3}. \tag{10}$$

The Lorentz index α represents the polarization state of the vector diquark. The two terms in Eq. (10) represent configurations consisting of a quark and either a spin-isospin zero (S) or a spin-isospin one (V) diquark, respectively. The couplings of the diquark with the quarks in a proton lead to the flavor functions

$$B_S = uS_{[u,d]}, \quad B_V = [uV_{\{u,d\}} - \sqrt{2}d\,V_{\{u,u\}}]/\sqrt{3}, \tag{11}$$

where the subscripts indicate the flavor content of the diquarks (S,V) in either antisymmetric or symmetric combinations. The DA $\varphi_{S(V)}(x_1)$, where x_1 is the momentum fraction carried by the quark, represents the light-cone wave function integrated over transverse momentum and is defined in such way that

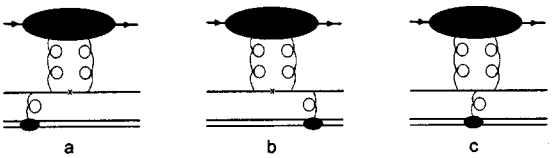

FIG. 2. Feynman graphs containing the 3-point diquark function (without 3-gluon coupling).

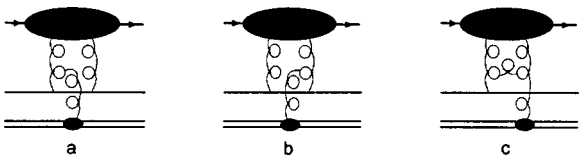

FIG. 3. Feynman graphs containing the 3-point diquark function (with 3-gluon coupling).

$$\int_0^1 dx_1\varphi_{S,(V)}(x_1) = 1. \tag{12}$$

The constant $f_{S(V)}$ acts as the value of the configuration space wave function at the origin.

The amplitude F_{+-} will be calculated in the spirit of the hard scattering approach [16] where the quarks and diquarks are connected by the minimal number of gluons, i.e., by three. Disconnected Feynman graphs are suppressed in the kinematical region of interest [16]. We also will employ several kinematical simplifications since we only consider the region $m^2 \ll |t| \ll s$. Color neutralization requires the t-channel exchange of two gluons. The third one is exchanged within one of the proton-proton vertices. Insofar our model for the flip amplitude bears resemblance to the Landshoff-Nachtmann [8] two-gluon model of the Pomeron. In contrast to [7] which refers to the standard nonflip Pomeron at small $-t$, in our approach the two gluons exchanged between the two proton-proton vertices do not only couple to one and the same constituent. This is not a contradiction since we are interested in a helicity flip amplitude at high energies and moderately large momentum transfer. The helicity flip amplitude can be expressed as a product of a helicity nonflip (HNF) vertex and flip (HF) vertex. The structure of the HNF vertex is shown in Fig. 1. For this vertex we only consider scalar diquarks in order to keep the model simple. The graphs contributing to the product of the HNF vertex and the HF vertex are shown in Figs. 2–5. To the HF vertex only vector diquarks contribute since, obviously, from scalar diquarks a helicity flip cannot be generated. The graphs shown in Figs. 2 and 3 contain 3-point diquark vertex functions while those shown in Figs. 4 (three-gluon interactions) and 5 (without three-gluon interactions) contain 4-point functions. In principle there is also a graph with a quartic gluon coupling. However, its contribution is suppressed at large s. It has been shown in [19] that this set of graphs leads to gauge-invariant scattering amplitudes. The n-point functions, indicated by blobs in Figs. 2–5, are given by a product of the relevant graphs for pointlike diquarks (see, for instance, Fig. 6) and appropriate phenomenological diquark form factors. These form factors take into account

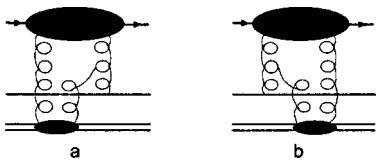

FIG. 4. Feynman graphs containing the 4-point diquark function (with 3-gluon coupling).

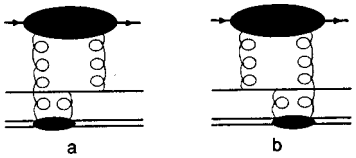

FIG. 5. Feynman graphs containing the 4-point diquark function (without 3-gluon coupling).

the composite nature of the diquarks. Since the 5-point functions provide only small corrections to the final results we omit them in our analysis.

The perturbative part of the diquark model, i.e., the coupling of gluons to diquarks follows standard prescriptions (for notations refer to [18])

$$SgS: ig_s t^a_{ij}(p_1+p_2)_\mu$$

$$VgV: -ig_s t^a_{ij}\{g_{\alpha\beta}(p_1+p_2)_\mu - g_{\mu\alpha}[(1+\kappa)p_1-\kappa p_2]_\beta - g_{\mu\beta}[(1+\kappa)p_2-\kappa p_1]_\alpha\}, \tag{13}$$

where $g_s=\sqrt{4\pi\alpha_s}$ is the QCD coupling constant. κ is the anomalous magnetic moment of the vector diquark and $t^a=\lambda^a/2$ the Gell-Mann color matrix. The couplings DgD are supplemented by appropriate contact terms required by gauge invariance, e.g.,

$$gSgS: -ig_s^2\{t^a t^b\}_{ij} g_{\mu\nu}. \tag{14}$$

The phenomenological diquark form factors are taken from [15,17]

$$F_S^{(3)}(Q^2)=\frac{Q_S^2}{Q_S^2+Q^2}; \quad F_V^{(3)}(Q^2)=\left(\frac{Q_V^2}{Q_V^2+Q^2}\right)^2; \tag{15}$$

$$F_S^{(4)}(Q^2)=a_S F_S^{(3)}(Q^2); \quad F_V^{(4)}(Q^2)=a_V\left(\frac{Q_V^2}{Q_V^2+Q^2}\right)^3. \tag{16}$$

The constants a_S and a_V are strength parameters introduced in order to take care of diquark excitation and breakup. These parametrizations are constrained by the requirement that asymptotically the diquark models evolves into the standard Brodsky-Lepage hard scattering model [16].

IV. THE STRUCTURE OF THE MODEL AMPLITUDE

According to our discussion in Sec. III the helicity flip amplitude can be expressed as a product of the helicity nonflip vertex to which only scalar diquarks contribute and the flip vertex that, in our model, is controlled by vector diquarks:

$$F_{+-}(s,t)=s\sqrt{-t}\frac{(4\pi)^3}{3t^2}f_S^2 f_V^2\int d\alpha_1 d\beta_1 \frac{\phi_S(\alpha_1)\phi_S(\beta_1)}{\alpha_1\alpha_2\beta_1\beta_2} \times \alpha_s(-\alpha_1\beta_1 t)\alpha_s(-\alpha_2\beta_2 t)F_S^{(3)}(-\alpha_2\beta_2 t) \times \int dx_1 dy_1 \phi_V(x_1)\phi_V(y_1)\sum_i C_i\hat{A}_i, \tag{17}$$

α_1 and β_1 denote the fractions of the baryon momentum carried by the quarks in the initial and final baryons entering the HNF vertex, respectively. $\alpha_2=1-\alpha_1$ and $\beta_2=1-\beta_1$ are the momentum fractions the diquarks carry. $x_1,(x_2),y_1(y_2)$ are the analogue quantities for the HF vertex. C_i is the color factor. To facilitate the discussion we split F_{+-} into contributions from various groups of Feynman graphs. The $\hat{A}_i$ are written as a contraction of the two tensors representing the HNF and HF vertices,

$$\hat{A}_i=H^{n.f.}_{\mu\nu}\cdot H^{\mu\nu}_{fi}. \tag{18}$$

The HNF vertex tensor has the simple form

$$H^{n.f.}_{\mu\nu}=\overline{u}(p_3+)[\gamma_\nu(p_1+p_3)_\mu+\gamma_\mu(p_1+p_3)_\nu]u(p_1,+). \tag{19}$$

The HF vertex tensors are to be calculated from the Feynman graphs shown in Figs. 2–6. They contain a factor of α_s with an appropriate argument (representing the virtuality of the internal gluon) and the vector diquark form factor besides the characteristics of the relevant Feynman graphs. We refrain from quoting the H^μ_{fi} explicitly but discuss the functions the functions $\hat{A}_i$ directly.

Figure 2a includes a propagator (marked by a cross) whose denominator contains a term proportional to s. Neglecting in this denominator terms proportional to t and m^2 in accordance with the condition $m^2,|t|\ll s$, we have

$$\hat{A}_{(2a)}=\hat{a}_{(2a)}(\alpha_1,\beta_1)\left[\frac{1}{sy_1(\alpha_1-\beta_1)+i\,\epsilon}+\frac{1}{-sy_1(\alpha_1-\beta_1)+i\,\epsilon}\right] =-\frac{2i\pi}{sy_1}\hat{a}_{(2a)}(\alpha_1,\alpha_1)\delta(\alpha_1-\beta_1), \tag{20}$$

where the regular function $\hat{a}_{2a}(\alpha_1,\alpha_1)$ is given in Table I. The contribution from Fig. 2b is given by $\hat{A}_{(2a)}(x_1,y_1)=\hat{A}_{(2b)}(y_1,x_1)$. There is a group of graphs in which the large variable s appears in two propagators denominators ($i=2c,3a,3b,4a,4b$):

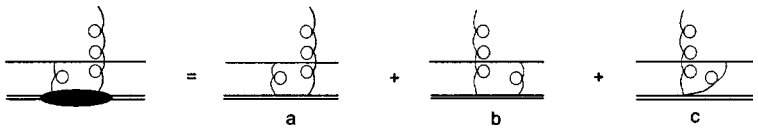

FIG. 6. Structure of the 4-point diquark function.

TABLE I. Color factors and of the functions d_{ij}, f_{ij} and $\hat{a}_i$ at $\beta_1=\alpha_1$ for sample graphs (for definitions see text). The contribution from graphs $4a$ and $5a$ is actually given for subgraph $6a$.

Figure	C_i	
2a	$\frac{8}{27}$	$\hat{a}_{(2a)}=-\frac{2s^2y_1\alpha_s(-x_2y_2t)\alpha_2[2(x_2+y_2)-\kappa(3x_1-2y_2)]}{tmx_2y_2}F_V^{(3)}(-x_2y_2t)$
3a	$\frac{i}{3}$	$\hat{a}_{(3a)}=\frac{-2s^2\alpha_s(-x_2y_2t)\alpha_2}{mx_2y_2}[2(x_2+y_2)(2y_1^2-y_1\alpha_2-2x_1y_1+2x_1\alpha_2+\alpha_1^2-1)-\kappa(5x_1^2+4y_1^3-10y_1^2+10y_1-5x_1^2y_1+3x_1y_1^2-4-3x_1y_1+4\alpha_1^2-5x_1^2\alpha_1-2x_1\alpha_1^2+2x_1\alpha_1+6y_1^2\alpha_1-2y_1\alpha_1^2-4y_1\alpha_1+x_1y_1\alpha_1)]F_V^{(3)}(-x_2y_2t)$
		$d_{(3a)1}=(\alpha_1-x_2)(\alpha_1-y_2)t+(x_2-y_2)^2m^2$
		$d_{(3a)2}=-(\alpha_1-y_2)\alpha_2t+y_1^2m^2,\ \ f_{(3a)1}=x_2-y_2,\ \ f_{(3a)2}=y_1$
4a	$\frac{i}{3}$	$\hat{a}_{(4a)}=\frac{s^2t\alpha_s(-x_2y_2t)\alpha_2\kappa(\alpha_1-y_1)(y_1-x_1)}{mx_1y_1m_V^2}[2y_2\alpha_1+4x_2\alpha_2+\kappa(3y_1\alpha_1-y_1-6\alpha_1^2+8\alpha_1+5x_1\alpha_1-4-5x_1)]F_V^{(4)}(-x_2y_2t)$
		$d_{(4a)1}=(\alpha_1-x_1)(\alpha_1-y_1)t+(x_1-y_1)^2m^2$
		$d_{(4a)2}=-(\alpha_1-y_1)\alpha_2t+y_2^2m^2,\quad f_{(4a)1}=x_1-y_1,\quad f_{(4a)2}=y_2$
5a	$\frac{8}{27}$	$\hat{a}_{(5a)}=\frac{2s^2t^2\alpha_s(-x_2y_2t)\alpha_1\alpha_2\kappa(y_2-\alpha_1)^2}{mm_V^2}[y_2\alpha_2+2x_2\alpha_1-\kappa(\alpha_1+y_2\alpha_2-3x_2\alpha_1+4\alpha_1^2)]F_V^{(4)}(-x_2y_2t)$
		$d_{(5a)1}=(\alpha_1-y_2)\alpha_1t+y_2^2m^2,\quad d_{(5a)3}=(\alpha_1-x_2)(\alpha_1-y_2)t+(x_2-y_2)^2m^2$
		$d_{(5a)2}=(y_2-\alpha_1)\alpha_2t+y_1^2m^2,\quad f_{(5a)1}=-y_2,\quad f_{(5a)2}=y_1,\quad f_{(5a)3}=x_2-y_2$

$$\hat{A}_i=\hat{a}_i(\alpha_1,\beta_1)\frac{1}{s(\alpha_1-\beta_1)f_{i1}+d_{i1}+i\epsilon_1}\times\frac{1}{s(\alpha_1-\beta_1)f_{i2}+d_{i2}+i\epsilon_2},\tag{21}$$

where f_{ij} and d_{ij} are functions of the momentum fractions α_1,β_1,x_1,y_1. Moreover, the d_{ij} depend on t and m^2 too. Obviously, these terms in the d_{ij} have to be kept now, otherwise the integrals in Eq. (17) would not exist. $\hat{A}_i$ can easily be integrated over β_1 by using partial fractioning and the standard formula

$$\frac{1}{z+i\epsilon}=\mathcal{P}\frac{1}{z}-i\pi\delta(z),\tag{22}$$

where $\mathcal{P}$ denotes the principal value integral. In the kinematical region of interest, namely $m^2,|t|\ll s$, the principal value part can be shown to be suppressed by $1/s$ as compared to the δ function part. The δ function provides the condition $\beta_1=\alpha_1+\mathcal{O}(1/s)$ in this case. Hence, to leading order in s, we approximate Eq. (21) by

$$\hat{A}_i\simeq-\frac{i\pi}{s}\hat{a}_i(\alpha_1,\alpha_1)\delta(\beta_1-\alpha_1)\times\left[\frac{\mathrm{signum}(f_{i1})}{d_{i2}f_{i1}-d_{i1}f_{i2}+i\epsilon\,\mathrm{signum}(f_{i1})}-\frac{\mathrm{signum}(f_{i2})}{d_{i2}f_{i1}-d_{i1}f_{i2}-i\epsilon\,\mathrm{signum}(f_{i2})}\right].\tag{23}$$

Representative examples of the functions d_{ij} and f_{ij} as well as of the $\hat{a}_i$ are quoted in Table I.

The other integrations appearing in Eq. (17) have to be done numerically using Eq. (22) again. Since in general signum(f_{i1}) is not equal to signum(f_{i2}) the $\hat{A}_i$ have both real and imaginary parts. An exception is Fig. 2c where $f_{(2c)1}=x_1$ and $f_{(2c)2}=y_1$. In this case the two principal value integrals cancel and the leading contribution to $\hat{A}_{2c}$ therefore it simplifies to

$$\hat{A}_{(2c)}\simeq-\frac{2\pi^2}{s}\hat{a}_{(2c)}(\alpha_1,\alpha_1)\delta(\alpha_1-\beta_1)\times\delta(d_{(2c)2}f_{(2c)1}-d_{(2c)1}f_{(2c)2}).\tag{24}$$

With the help of this new δ function a second integration in Eq. (17) can be immediately carried out.

Figures 5a and 5b, comprising 4-point diquark vertex functions, have s in three propagators. The contribution of these graphs can be written in the form

$$\hat{A}_i=\hat{a}_i(\alpha_1,\beta_1)\prod_{j=1}^{3}\frac{1}{s(\alpha_1-\beta_1)f_{ij}+d_{ij}+i\epsilon_j}.\tag{25}$$

As an example we quote the functions $\hat{a}_{5a}$ for Fig. 5a together with the $d_{(5a)j}$ and $f_{(5a)j}$ in the table. To leading order in s these contributions are also dominated by the imaginary parts of the propagator poles at $-d_{ij}/(sf_{ij})$. Up to corrections of order $1/s$ this again implies $\beta_1=\alpha_1$. Thus, we find for $i=5a,5b$

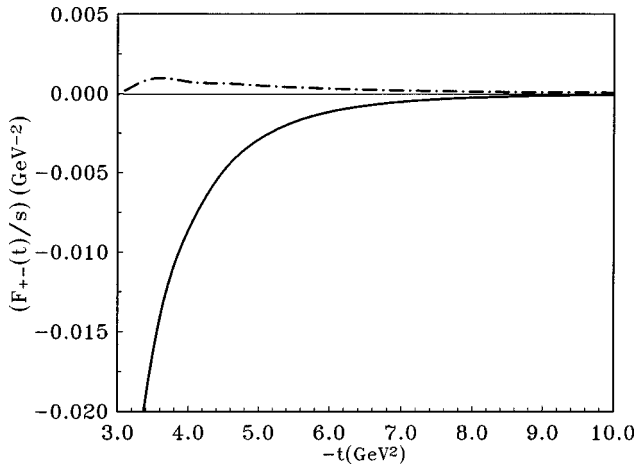

FIG. 7. t dependence of the F_{+-} amplitude at $s=100$ GeV^2, solid line-imaginary part; dot-dashed line-real part.

$$\hat{A}_i \simeq -\frac{i\pi}{s}\hat{a}_i(\alpha_1,\alpha_1)\,\delta(\alpha_1-\beta_1) \times\Bigg[\frac{\text{signum}(f_{i1})}{d_{i2}f_{i1}-d_{i1}f_{i2}+i\,\text{signum}(f_{i1})\epsilon_2} \times\frac{1}{d_{i3}f_{i1}-d_{i1}f_{i3}+i\,\text{signum}(f_{i1})\epsilon_3}+(1,2,3)\ \text{cyclic}\Bigg]. \tag{26}$$

How to proceed from here should be obvious.

Finally let us discuss Fig. 3c. A pole only appears in the s-channel propagator and $\hat{A}_{(3c)}$ is of the form

$$\hat{A}_{(3c)}=\hat{a}_{(3c)}\frac{1}{s(\alpha_1-\beta_1)(y_1-x_1)+d_{(3c)}+i\epsilon}. \tag{27}$$

It can be shown that the leading log contribution from this graph to the integral over y_1,β_1 in Eq. (17) is dominated by the region near $\alpha_1=\beta_1$ and $y_1=x_1$:

$$\int_0^1 dy_1\int_0^1 d\beta_1\frac{F(s,t,\beta_1,y,\dots)}{s(\alpha_1-\beta_1)(y_1-x_1)+d_{(3c)}+i\epsilon} \sim F(s,t,\beta_1=\alpha_1,y_1=x_1\dots)I(s), \tag{28}$$

where F absorbs all terms appearing in Eq. (17) including $\hat{a}_{(3c)}$ and

$$I(s)=\int_0^1 dy_1\int_0^1 d\beta_1\frac{1}{s(\alpha_1-\beta_1)(y_1-x_1)+d_{(3c)}+i\epsilon}. \tag{29}$$

Approximately this integral is given by

$$I(s)\sim\int_{-1/2}^{1/2}du\int_{-1/2}^{1/2}dv\frac{1}{suv+d_{(3c)}+i\epsilon}+\mathcal{O}(1/s) =\frac{2}{s}\left[\text{dilog}\left(\frac{-s}{4d_{(3c)}}\right)-\text{dilog}\left(\frac{s}{4d_{(3c)}}\right)\right]\sim-\frac{2i\pi}{s}\ln s. \tag{30}$$

Note, that $\hat{a}_{(3c)}\propto s^2$ as the contributions from the other graphs (see the table). Thus, the dominant contribution from Fig. 3c is

$$(F_{+-})^{LL}_{(3c)}\propto is\ln(s)f(t). \tag{31}$$

We calculate numerically in Eq. (28) not only the leading $s\ln s$ term but also the nonlogarithmic contribution which behave like s.

V. NUMERICAL RESULTS FOR SPIN-DEPENDENT *pp* SCATTERING

In our numerical studies of proton-proton scattering we use the following form of the scalar and vector diquark DA:

$$\varphi_S(x_1)=N_S x_1x_2^3\exp[-b^2(m_q^2/x_1+m_S^2/x_2)],$$
$$\varphi_V(x_1)=N_V x_1x_2^3(1+5.8x_1-12.5x_1^2) \times\exp[-b^2(m_q^2/x_1+m_V^2/x_2)] \tag{32}$$

and the set of parameters

$$f_S=73.85\ \text{MeV},\quad Q_S^2=3.22\ \text{GeV}^2,\quad a_S=0.15,$$
$$f_V=127.7\ \text{MeV},\quad Q_V^2=1.50\ \text{GeV}^2,\quad a_V=0.05, \tag{33}$$
$$\kappa=1.39$$

as proposed in [17,18]. The values of the masses in the exponentials are taken as 330 MeV (for the quarks) and 580 MeV (for the diquarks). The transverse size parameter b is taken to be 0.498 GeV^{-1}. The normalization constants N_S and N_V have the values 25.97 and 22.29, respectively. As we mentioned in the preceding section the β_1 integration is trivial. The other three integrations over the hard amplitude and the proton DAs are carried out numerically. Since we neglect $1/s$ corrections throughout we find an energy independent ratio of the helicity flip and nonflip amplitudes.

Let us discuss the role of the contributions from the individual graphs briefly. The contributions from Figs. 2a and 2b to F_{+-} are purely imaginary. Thus, although these contributions lead to helicity flips they do not produce a phase difference between the F_{+-} and F_{++} and, hence, do not contribute to the single spin asymmetry. Figure 2c yields a real contribution that is quite small, about a few percent of Im F_{+-} at $|t|\leqslant 10$ GeV^2. The contributions to the real part of F_{+-} provided by Figs. 3a and 3b though substantial are compensated by the contribution from Fig. 3c to a large extent. The contributions of Figs. 4a, 4b, 5a and 5b, to the real part of F_{+-} are very small as the numerical evaluation re-

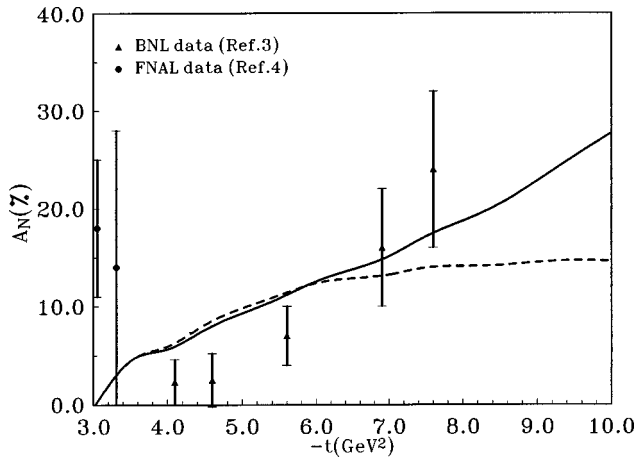

FIG. 8. Model predictions for single-spin asymmetry at $s=100$ GeV^2 [solid line for the MPE model (8); dashed line for the LP model (9)].

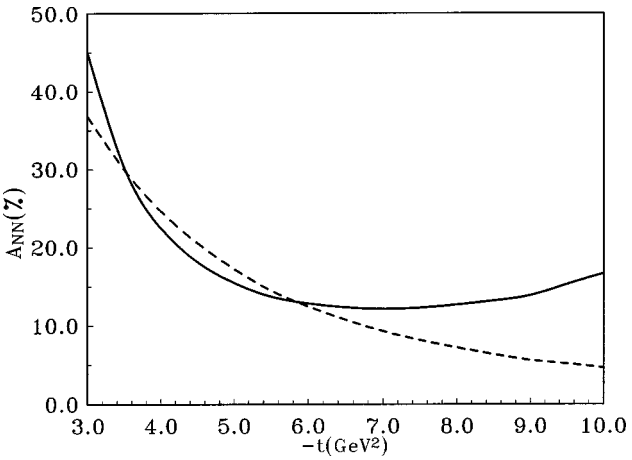

FIG. 9. Model predictions for double-spin asymmetry at $s=100$ GeV^2 [solid line for the MPE model (8); dashed line for LP model (9)].

veals. Their imaginary parts, however, are not small as is that from Fig. 3c. These imaginary contributions play an important role for the double spin asymmetry parameter A_{NN}.

The results of our calculations for the helicity flips amplitude F_{+-} are shown in Fig. 7 for $s=100$ GeV^2. As can be seen from that figure the imaginary part of F_{+-} is much larger than its real part. The real part of F_{+-} changes sign at $|t|\sim 3.5$ GeV^2. The absolute value of the ratio of helicity flip and nonflip amplitudes is fairly large $|F_{+-}|/|F_{++}|\sim 0.2-0.3$ at $|t|\geqslant 3$ GeV^2 indicating the substantial amount of helicity flips generated through the vector diquarks in our model.

The interference of the real part of F_{+-} with the purely imaginary ansatz for the amplitude F_{++} yields the single-spin asymmetry A_N (5). Our prediction for A_N at $s=100$ GeV^2 and for $|t|\geqslant 3$ GeV^2 is shown in Fig. 8 and compared to the only available experimental data in that region (at $s=370$ GeV^2) [4]. The quality of the present data is poor and prevents any severe test of our predictions. The predicted asymmetry amounts to about 20–30 % for $|t|>6$ GeV^2; it is of the same order of magnitude as has been observed in the low-energy BNL experiment [3]. The decrease of the asymmetry at smaller momentum transfer is connected with the smallness of $\mathrm{Re}\,F_{+-}$ near $|t|=3$ GeV^2.

The predictions for the double spin asymmetry A_{NN} are shown in Fig. 9. A_{NN} turns out to be of the order of 10–20 %. Our results for the spin asymmetries are rather close to those obtained in [13,24] although the latter are valid in the momentum transfer region 2 GeV$^2<|t|<4$ GeV^2. The spin observables obtained within the model are essentially independent on the parametrizations (8,9) used for the nonflip amplitude F_{++}.

VI. SUMMARY

On the basis of the diquark model we have calculated spin effects in high-energy proton-proton scattering at moderately large momentum transfer. The two-gluon graphs for the color-singlet *t*-channel exchange have been considered for the helicity flip amplitude while for the helicity nonflip amplitude a phenomenological parametrization is used. It describes qualitatively the differential cross section of the elastic pp scattering. The F_{+-} amplitude is calculated under the assumption that the *t*-channel gluons couple to one constituent, quark or diquark, each in the helicity nonflip vertex. In the helicity flip amplitude we include the perturbative α_s correction. Hence, we consider minimally connected graphs which allow us to keep all constituents collinear. In our model the helicity flips are generated by vector diquarks. It turns out that the flip amplitude F_{+-} is of substantial magnitude and not in phase with the nonflip contribution.

Our model, therefore, provides a single-spin asymmetry that is rather large for momentum transfer $|t|\geqslant 3$ GeV^2. The double spin transverse asymmetry in this kinematical region are rather large in our model. The important feature of the spin effects obtained in our model is their weak energy dependence. On the other hand, they decrease with increasing momentum transfer. Our results are valid at large *s* and moderately large momentum transfer ($>$few GeV^2). This kinematical region can be investigated for instance in the proposed DESY HERA-$\vec{N}$ experiment [25].

Finally we want to stress that our predictions for A_N should not be taken literally since phase differences are hard to calculate; they depend on many subtle details which are not well under control in a model. The diquark model on which our model is based was designed for a different kinematical region. In so far, a failure of our prediction for A_N would not necessarily imply a failure of the diquark model in general but would rather indicate that the phase differences are not well under control and/or that the diquark model is applied beyond its range of applicability.

ACKNOWLEDGMENTS

We would like to thank J. Bolz, A. Efremov, R. Jakob, and O. Nachtmann for fruitful discussions. S.V.G. would like to thank the Fachbereich Physik, Universität Wuppertal, for the warm hospitality in Wuppertal. This work was supported in part by the Heisenberg-Landau Grant.

[1] A.V. Efremov and O.V. Teryaev, Phys. Lett. **150B**, 383 (1985).

[2] S.B. Nurushev, in Proceedings of the 2nd International Workshop on High Energy Spin Physics, Protvino, Russia, 1984 (Serpukhov, 1985), p. 5; A.D. Krisch, in Proceedings of the 6th International Symposium on High Energy Spin Physics, Marseille, France, 1984, edited by J. Soffer [J. Phys. (France) **46**, C2-511 (1985)].

[3] D. C. Peaslee *et al.*, Phys. Rev. Lett. **51**, 2359 (1983); A.D. Krisch, in *Proceedings of the Conference on High Energy Spin Physics*, Bonn, Germany, 1990, edited by K.H. Althoff and W. Meyer (Springer-Verlag, Berlin, 1991), p. 20.

[4] G. Fidecaro *et al.*, Phys. Lett. **105B**, 309 (1981).

[5] N. Akchurin, N.H. Buttimore, and A. Penzo, Phys. Rev. D **51**, 3944 (1995).

[6] F.E. Low, Phys. Rev. D **12**, 163 (1975); S. Nussinov, Phys. Rev. Lett. **34**, 1286 (1975).

[7] A. Donnachie and P.V. Landshoff, Nucl. Phys. **B244**, 322 (1984).

[8] P.V. Landshoff and O. Nachtmann, Z. Phys. C **34**, 405 (1987).

[9] M. Diehl, Eur. Phys. J. C **6**, 503 (1999).

[10] S.V. Goloskokov, Phys. Lett. B **315**, 459 (1993).

[11] S.V. Goloskokov, Phys. Rev. D **53**, 5995 (1996); in *Proceedings of 12th International Symposium on High Energy Spin Physics*, Amsterdam, 1997, edited by K.W. de Jager *et al.* (World Scientific, Singapore, 1997), p. 334, hep-ph/9610342; Proceedings of the 1997 Workshop Deep Inelastic Scattering off Polarized Targets: Theory Meets Experiment, edited by J. Blümleim, A. De Roeck, T. Gehrmann, and W.-D. Nowak, Report No. DESY 97-200, p. 674, hep-ph/9710293.

[12] C. Bourrely, J. Soffer, and T.T. Wu, Phys. Rev. D **19**, 3249 (1979).

[13] S.V. Goloskokov, S.P. Kuleshov, and O.V. Selyugin, Z. Phys. C **50**, 455 (1991).

[14] G. Bunce *et al.*, Phys. World **3**, 1 (1992); W.-D. Nowak, in *High Energy Spin Physics*, AIP Conf. Proc. No. 343, edited by K.J. Heller and S.L. Smith (AIP, New York, 1995), p. 412; W. Guryn *et al.*, PP2PP Proporsal to measure total and elastic pp-scattering at RHIC, Brookhaven, New York (1993).

[15] M. Anselmino, P. Kroll, and B. Pire, Z. Phys. C **36**, 89 (1987); P. Kroll, in *Proceedings of the Adriatic Research Conference on Spin and Polarization Dynamics in Nuclear and Particle Physics*, Trieste, Italy, 1988, edited by A.O. Barut and A. Penzo (World Scientific, Singapore, 1990), pp. 108–112.

[16] S.J. Brodsky and G.P. Lepage, Phys. Rev. D **22**, 2157 (1980).

[17] P. Kroll, W. Schweiger, and M. Schürmann, Int. J. Mod. Phys. A **6**, 4107 (1991); P. Kroll, Th. Pilsner, M. Schürmann, and W. Schweiger, Phys. Lett. B **316**, 546 (1993); P. Kroll, M. Schürmann, and P.A.M. Guichon, Nucl. Phys. **A598**, 435 (1996); P. Kroll, M. Schürmann, K. Passek, and W. Schweiger, Phys. Rev. D **55**, 4315 (1997).

[18] R. Jakob, P. Kroll, M. Schürmann, and W. Schweiger, Z. Phys. A **347**, 109 (1993).

[19] R. Jakob, Phys. Rev. D **50**, 5647 (1994); Interner Bericht, Report No. WUB-DIS 93-12, Wuppertal, Germany, 1993.

[20] G.P. Ramsey and D. Sivers, Phys. Rev. D **47**, 93 (1993).

[21] P.V. Landshoff, Phys. Rev. D **10**, 1024 (1974).

[22] P.D.B. Collins and E.J. Squires, *Regge Poles in Particle Physics*, Springer Tracts in Modern Physics, Vol. 45 (Springer-Verlag, Berlin, 1968).

[23] E. Nagy *et al.*, Nucl. Phys. **B150**, 221 (1979).

[24] S.V. Goloskokov and O.V. Selyugin, Yad. Fiz. **58**, 1894 (1995) [Phys. At. Nucl. **58**, 1791 (1995)].

[25] M. Anselmino *et al.*, in Proceedings of the Workshop on Future Physics at HERA, DESY, Hamburg, Germany, 1996, edited by G. Ingelman, A. De Roeck, and R. Klanner, Report No. DESY 96-235, p. 837.